THE ROLE OF POROSITY IN EXTERNAL SULPHATE ATTACK

Tai Ikumi[a],*, Sergio H. P. Cavalaro[b] and Ignacio Segura[a, c]

[a] Department of Civil and Environmental Engineering, Universitat Politècnica de Catalunya, Barcelona Tech, Jordi Girona 1-3, C1, E-08034 Barcelona, Spain
[b] School of Architecture, Building and Civil Engineering, Loughborough University, Leicestershire, LE11 3TU, United Kingdom
[c] Smart Engineering, Jordi Girona 1-3 K2M 202c, Barcelona, Spain

* Corresponding author: Tai Ikumi. Department of Civil and Environmental Engineering, Universitat Politècnica de Catalunya Barcelona Tech, Jordi Girona 1-3, C1, E-08034 Barcelona, Spain. Email address: tai.ikumi@upc.edu, Tel: +34 93 401 6507 Fax: +34 93 401 1036

ABSTRACT

Design codes promote a limitation of permeability (indirectly of porosity) to reduce the sulphate ingress and improve the resistance of concrete and mortar to external sulphate attack (ESA). However, porosity could also have a positive effect on durability by generating additional space to accommodate the expansive phases. The aim of this study is to evaluate the role of porosity in ESA. For that, changes at the macro-scale, phase composition and pore network are monitored for mortar compositions with different pore-size distribution. Results indicate the existence of two mechanisms: the capacity to accommodate expansive phases controls the durability during the initial stages of the attack, while at later stages durability is defined by the permeability. Results from specimens with air-entrainer suggest that the intentional increase of porosity towards maximising the capacity to accommodate expansive products might be a valid approach in order to reduce the expansive forces generated during ESA.

Keywords: Sulphate Attack (C), Ettringite (D), X-Ray Diffraction (B), Mercury Porosimetry (B), Pore structure

1. INTRODUCTION

External sulphate attack (ESA) is a complex degradation process that can compromise the long-term durability of cement-based materials in contact with sulphate-rich environments. ESA requires the penetration of sulphate ions from an external source into the cementitious material. The connection between the external aqueous media and the pore solution alter the equilibrium conditions in the liquid system, leading to a net mass flow and subsequent chemical reactions to restore a minimum energy state. The chemical reactions triggered define the damage mechanism associated with the attack. ESA caused by sodium sulphate is characterised by ettringite and gypsum formation in such a quantity that the material sustains chemical and physical damage. Chemical damage refers to the degradation of mechanical properties in the cementitious matrix caused by the decalcification of hydrated phases, while physical damage is usually related to the degradation caused by expansive forces generated at the pore-level. These forces are ultimately responsible for the development of expansions and possible cracking and spalling [1,2].

There is still controversy on how ettringite and gypsum formation are converted into actual expansions. The prevailing theories are the volume increase approach and the crystallisation pressure theory. The first assumes that the expansions observed are the result of the additional volume generated by the expansive products precipitated during the attack (e.g. [3]). Therefore, the amount of ettringite precipitated determines the magnitude of the expansions. The latter states that expansions are caused by the crystallisation pressure exerted on the pore walls due to the formation of ettringite [4,5]. In this case, ettringite has to be growing from a supersaturated solution in confined conditions in order to convert the chemical energy into mechanical work, meaning that not all ettringite contributes to the expansions. Recent investigations place the crystallisation pressure theory as the most plausible, with it currently the most accepted mechanism of damage [6]. A comprehensive review of the main suggested theories can be found in [2].

Building and structural codes specify precautionary measures when obtaining sulphate-resisting concrete. These measures consist of limiting the aluminate content in the cement, using low water/cement ratios to reduce the permeability and increasing of compressive strengths to resist the internal stress caused by the expansion (e.g. Model Code 2010, BS 8500-1:2006, ACI 201.2R-08, UNE EN 206-1:2008). The recommendation of low permeability seeks to reduce the penetration of external aggressive ions into the inner layers of the material, with several studies supporting such a recommendation. Nowadays, it is accepted that cement-based materials with low permeability show a better durability against sulphates than the corresponding samples with higher permeability (e.g. [1,2,7-10]). Although permeability and porosity are not synonyms, in general the fall-off in permeability is accompanied by a consequent decrease in the porosity of the matrix. Therefore, the limitation of permeability usually indirectly implies a reduction of the porosity provided by the pore network.

However, the role of the pore network during the attack is not only related to the transport of sulphate ions. Since pores are basically empty spaces within a rigid matrix, they have a certain capacity to accommodate expansive phases before creating damage. In this context, pores might act as deposits or containers of the expansive products precipitated during ESA. This phenomenon has been described by other authors [3,11-13] as the buffer capacity of the matrix and it is directly or indirectly considered in both damage mechanisms previously mentioned.

Some studies report trends that may suggest the positive consequence of a highly porous material in comparison with a dense matrix with low permeability and porosity. Naik et al. [14] found that a reduction of the water/cement ratio caused more severe physical damage in samples exposed to a sodium sulphate solution. The authors attributed the earlier damage and the more rapid failure of the samples to the reduced extensibility of the material and the low capacity of the dense pore network to accommodate expansive phases [14]. M. Santhanam et al. [15,16] assessed the behaviour of mortars with a presumably high capacity to accommodate expansive phases by the use of an air-entrainer admixture. The authors obtained delayed levels of deterioration in such mortars, suggesting that entrained air might provide sites for nucleation of expansive phases, which might in turn lead to a reduced damage in the paste. Another hypothesis formulated was that air might help arresting the growth of cracks due to their spherical shape.

Despite that, solid evidence and explanations regarding the contribution of a highly porous matrix are rare and inconclusive. Consequently, the maximisation of the buffer capacity of the matrix by increasing the porosity has not been recognised as a possible approach to obtain more durable materials against ESA.

The objective of this study is to assess the influence of the pore network on the durability against ESA. For that, mortar compositions with different porosities (from 8.1 % to 18.8 %) are subjected to accelerated sulphate attack. In order to isolate the effects of porosity, C_3A content, external sulphate concentration and geometrical characteristics of samples are kept constant for all compositions. Characterisation of the macro-scale behaviour is performed by monitoring the dimensional, mass and ultrasonic velocity variation over time. Changes in phase composition are investigated by X-ray diffraction (XRD) and evolution of the pore characteristics of the mortars are examined by mercury intrusion porosimetry (MIP).

This study provides evidences and explanations that help understanding the role of porosity in samples subjected to ESA. The findings might open up alternative strategies for the future design of durable cementitious materials against the attack.

2. EXPERIMENTAL PROGRAMME

2.1 MATERIALS AND MORTAR COMPOSITIONS

Portland cement (CEM I 52.5R) with high C_3A content was used in order to promote ettringite formation and the potential damage during ESA. Table 1 shows the chemical (determined by XRF spectrometry) and mineralogical (estimated using Bogue equations) composition and summarises the physical properties of the cement. Data provided by Bogue equations is only used to classify the cement as highly reactive under sulphate exposure. De-ionised water and siliceous sand following the specifications of UNE-EN 196-1:2005 were used in all mortars. Commercial superplasticiser GLENIUM ACE 456 and air-entrainer MasterAir 100 were added to the mixtures.

Table 1. Chemical and mineralogical composition of the Portland cement.

Chemical composition [% bcw*]	
SiO_2	19.5
Al_2O_3	5.9
Fe_2O_3	1.7
CaO	63.1
MgO	2.1
SO_3	3.5
K_2O	0.8
Na_2O	0.4
Cl^-	-
LOI	3.0
Phase composition [% bcw*]	
C_3S	65.4
C_2S	10.6
C_3A	12.3
C_4AF	5.6
Physical properties	
Spec. surf. area (BET) [m^2/g]	1.10

d_{10} [μm]	0.58
d_{50} [μm]	6.88
d_{90} [μm]	31.84

bcw: by cement weight

Table 2 shows the composition of the four matrices included in this study. Different degrees of refinement of the pore network were obtained by varying the water/cement ratio from 0.38 to 0.55 and by using an air-entrainer. Initial reference porosities obtained by MIP test at 14 days after sulphate exposure are included in Table 2. The different compositions considered cover a wide range of porosities (from 8.1 % to 18.8 %). The nomenclature adopted for each composition follows the pattern *water/cement ratio – initial porosity*. Air-entrained mortars have the term '*AE*' prior to the water/cement ratio. Notice that the cement content remained constant for all compositions, ensuring similar amount of C_3A and potential expansion. Therefore, the macro-scale response of mortars after sulphate exposure can be associated mainly to differences in the pore system.

The mixing procedure defined in UNE-EN 196-1:2005 was adopted, introducing small modifications to cover the specificities of the admixtures added. The air-entrainer was added at the end of the mixing procedure and mixed at high speed for 60 seconds. The superplasticiser was mixed with the de-ionised water in contents to assure flow extents of 20 cm ± 0.5 cm. This flow extent was defined to favour similar workability and surface finish amongst all mortar compositions.

Table 2. Compositions and mass attenuation coefficient (MAC) of the mortars.

Material	0.38_8.1%	0.45_12.4%	0.55_13.7%	AE0.45__18.8%
Cement [kg/m^3]	580	580	580	580
Sand [kg/m^3]	1425	1325	1180	1325
Water [kg/m^3]	220	261	319	261
Air-entrainer [% bcw]	-	-	-	0.3
Superplasticiser [% bcw]	1.00	0.50	-	0.25
Water/cement ratio	0.38	0.45	0.55	0.45
Porosity [%]	8.1	12.4	13.7	18.8
MAC [cm^2/g]	48.11	48.01	47.84	48.01

2.2 EXPERIMENTAL PROCEDURE

2.2.1 SPECIMEN PREPARATION

Ø78 mm x 17 mm mortar specimens were cast to conduct this study. Such geometry was chosen to avoid the typical corner spalling observed in rectangular samples that might alter the macro-scale response during the attack [17]. The dimensions selected maintain similar exposed surface-volume ratio than other studies that showed good balance between test duration and representativeness [18]. Due to the importance of the surface finish in transport-related degradation processes, specimens were cast in individual moulds to obtain external surfaces representative of field conditions and to avoid the presence of cut aggregates on the exposed surfaces.

Figure 1 shows a schematic representation of the moulds and the casting process adopted. The moulds comprised a PE rigid base with four fixed PVC pipes and a movable PE rigid cover. Top and side views of these components are shown in Figure 1a. Five Ø12 mm x

160 mm bolts were used to guide the cover into the base during assembly (Figure 1b), while twelve PE bars were used to fix the PVC pipes and block the cover at a specific height to obtain a sample thickness of 17 mm. To relieve the excess mortar, purge exits were introduced in the cover. Before assemblage, the mortar (represented in light hatching) was first poured inside the PVC pipes and compacted with 15 jolts in the flow table (ASTM C1437) at a rate of one jolt per second to eliminate air pockets. After that, the cover was placed and tightened to the base. In order to ensure adequate surface finish quality, the moulds were then vibrated for ten seconds at the vibration table. Finally, the hex nuts were further tightened until the cover reached the PE bumpers that control the height of the specimens.

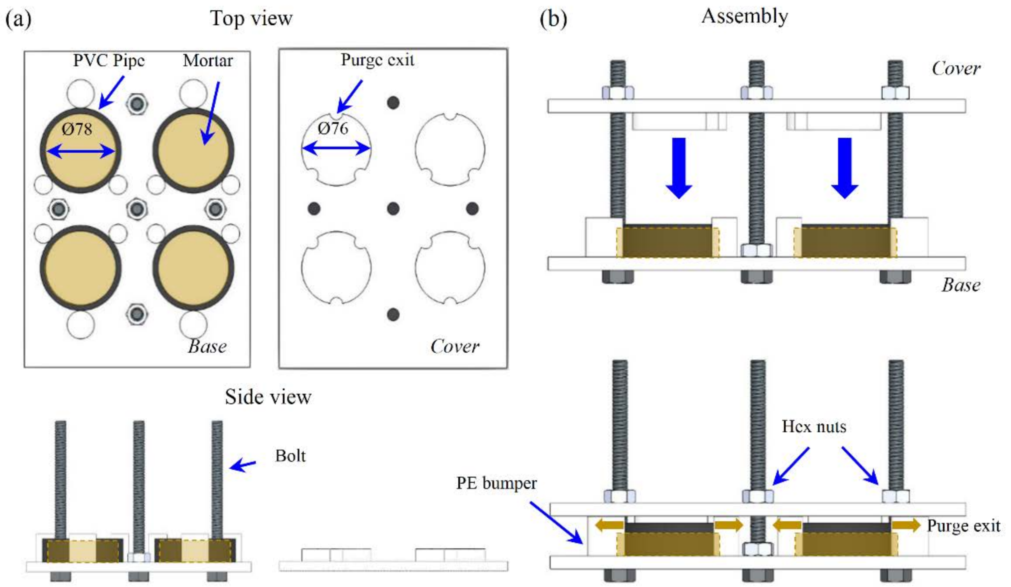

Specimens were demoulded 24 hours after casting and the lateral surface was water-sealed with MasterSeal M 338 flexible epoxy coating to ensure linear penetration of the sulphate ions through the two main surfaces of the specimen. Figure 2a shows a final specimen obtained after applying the coating. Once sealed, all specimens were cured in water at 25 ºC ± 1 ºC for 24 hours. Then, they were placed laterally inside plastic containers and submerged in a sulphate-rich water solution (Figure 2b).

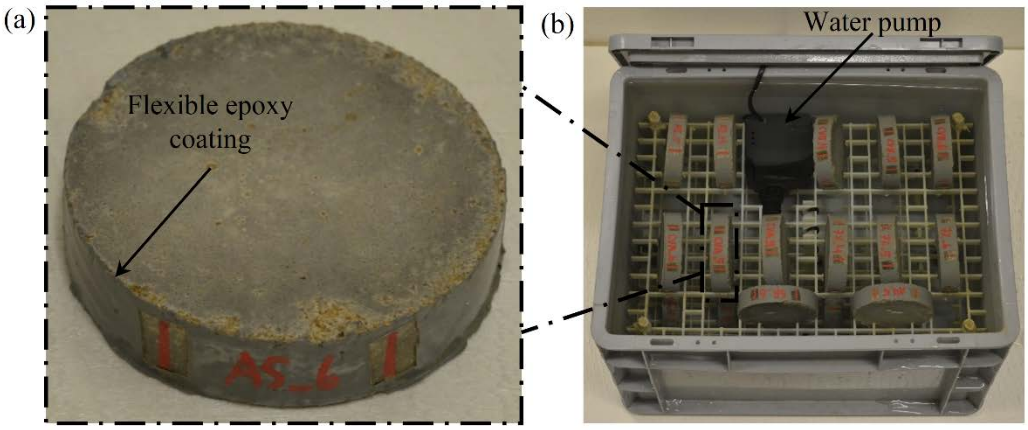

2.2.2 EXPOSURE CONDITIONS

Specimens were exposed to the sulphate solution shortly after casting to reproduce the real exposure conditions of most structures subjected to ESA, which are usually built *in situ*. Sulphate concentration of 30 g of Na_2SO_4/l was used to accelerate the degradation process [19]. The solution was renewed weekly during the first month and every other week until the end of the test at 365 days. The volumetric ratio of sulphate solution to mortar was 12, a level that should be representative of field conditions where the material is exposed to continual supply of sulphate ions.

Water pumps were placed inside the plastic containers to ensure a continuous flow from the bottom to the top in order to minimise concentration gradients (Figure 2b). The containers were filled to the top and covered to reduce contact with the air, thus limiting CO_2 dissolution and carbonation. Reference samples of each composition were also exposed to non-aggressive curing with water without sulphates for comparative purposes.

2.2.3 TEST METHODS

- *Macro-structural monitoring*

Characterisation of the macro-scale behaviour relies upon measurements of expansion, mass and ultrasonic velocity and visual inspection of the specimens. All measurements were taken weekly during the first month and every other week until the end of the study. The values presented in this study are the average of three specimens.

Due to the singular shape of the specimens, a device was designed to measure the radial free expansions of the mortars (Figure 3a), which consisted of a MICROMASTER electronic micrometer with a precision of ± 0.001 mm and a metallic platform to fix the measured points. Several vertical strips were introduced to facilitate the measuring and to guarantee a similar position of the specimens (Figure 2a). Prior to the start of the experimental programme, the precision of the equipment was evaluated during a series of over 500 measurements on mortar specimens with and without gauge studs. Specimens with gauge studs obtained higher variability of the measurements (± 0.008 mm with studs and ± 0.002 mm without studs). Consequently, the use of studs was discarded. For each specimen, three radial directions were measured at each time to cover all the sample (Figure 3b). Therefore, each expansion value presented in this study is the average of nine measurements.

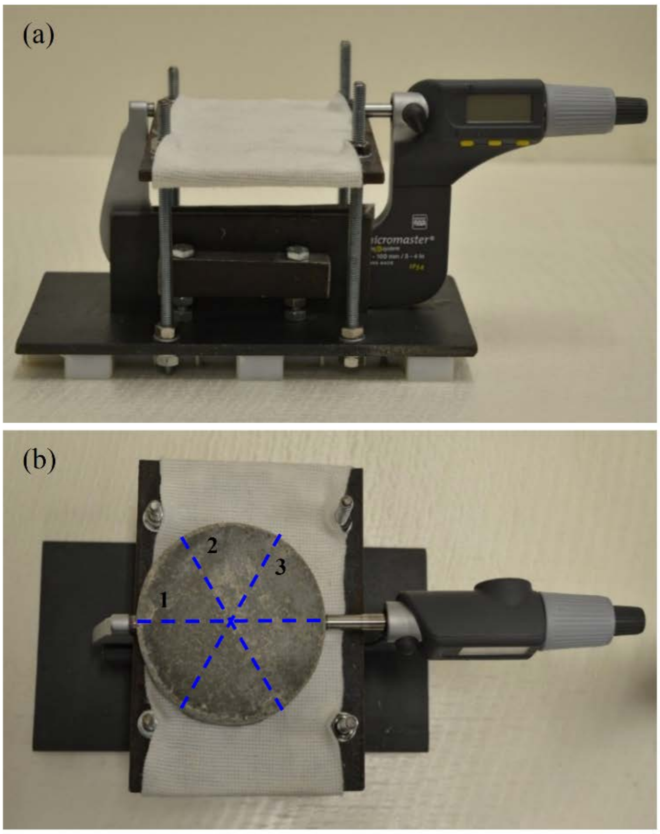

The ultrasonic pulse velocity between the two exposed faces was measured at 500 kHz sampling frequency using a PUNDIT PL-200, while a zero-crossing algorithm was used to calculate the travelling time of the ultrasonic wave. Mass evolution was controlled with a precision balance of ±0.01 g. Surface water of the samples was dried up before weighting.

- *Phase composition evolution*

Changes in phase composition were examined using X-ray diffraction (XRD) at 28, 90, 180, 270 and 365 days. Samples for XRD were core-drilled from original specimens using a column drill equipped with a water-cooled diamond drill bit [20]. For each composition, samples were extracted from the same specimens to reduce the variability of the results. Due to the symmetric sulphate exposure conditions, each sample was divided in two. One half was crushed and the powder was pressed in cylindrical standard sample holders of 16 mm diameter and 2.5 mm height, while the other half was discarded. XRD measurements were made using a PANalytical X'Pert PRO MPD Alpha1 Θ/2Θ diffractometer in reflection Bragg Brentano geometry of 240 mm of radius. $CuK_{\alpha1}$ radiation (λ=1.5406 Å) and X'Celerator detector with active length of 2.122 ° were used. Work power was set to 45 kV – 40 mA. Θ/2Θ scans from 4 to 80 º2Θ with a step size of 0.017 º2Θ and a measuring time of 50 seconds per step were performed. Sample holders were spun at two revolutions per second.

Rietveld analysis using the external standard method was performed on the XRD results for the quantitative study of the crystalline phases. The external standard method was used for quantification instead of the more common internal standard method to avoid homogenisation problems and further dilution of the cement paste in the analysed sample [21-23]. The adopted methodology is similar to earlier works [21-23]. Phase weight fractions were calculated from phase scale factors by comparison to the scale factor of the external standard (Al_2O_3), measured under identical diffractometer conditions. The density and volume values of the unit cell of each phase were obtained from data sets from ICSD. Mass attenuation coefficients (MAC) of the different compositions used were calculated from the MAC of each component, including the water content and taking into account the weight fraction of each one. Final MAC of the different mortars used are listed in Table 2.

All Rietveld refinements were carried out with X'Pert High Score Plus software package by PANalytical, using the structures listed in Table 3. Small peaks of Fe-substituted ettringite formed as a result of the reaction between sulphate ions and the ferroaluminate phases were detected in some mortars at late stages of the attack. Since its crystalline structure for Rietveld refinement was not available it was not considered during quantification. The global variables refined were the background polynomial with 4 coefficients (1st, 2nd, 3rd and 5th) and the zero shift. For all phases detected, individual scale factors and lattice parameters were refined. A pseudo-Voigt function was chosen to model the peak shape. The phase profile width (*w*) was refined for quartz, ettringite, portlandite and gypsum. For quartz and portlandite, the profile parameters *U*, *V* and the peak shape were also refined. Preferred orientation corrections were applied when necessary for gypsum (0 2 0), portlandite (0 0 1), ettringite (1 0 0) and quartz (1 0 1) as long as the phase content was above 2%.

Table 3. Phase structures used for Rietveld refinement.

Phase	Chemical composition	ICSD Code	Reference
Alite	Ca_3SiO_5	94742	[24]
Belite_o	Ca_2SiO_4	81097	[25]
Portlandite	$Ca(OH)_2$	15471	[26]
Calcite	$CaCO_3$	79673	[27]
Ettringite	$Ca_6Al_2(SO_4)_3(OH)_{12}26H_2O$	155395	[28]
Gypsum	$CaSO_42H_2O$	15982	[29]
Ferrite	Ca_2AlFeO_5	9197	[30]
Quartz	SiO_2	200721	[31]
Corundum	Al_2O_3	73725	[32]

- *Pore system evolution*

Evolution of the pore system of the mortars were examined through mercury intrusion porosimetry (MIP) with a Micrometrics AutoPore IV 9500 (contact angle 140º and Hg surface tension 485 dynes/cm) at 14, 28, 91, 180 and 270 days. Tests after 270 days were not performed due to the spalling of the external layer of the sample during drilling. Samples were extracted following the same procedure as described in the previous section. Due to the symmetric sulphate exposure conditions, each sample was divided in two halves and analyzed separately, before the samples were freeze-dried to ensure full desaturation prior to mercury intrusion.

3. RESULTS AND DISCUSSION

3.1 MACRO-STRUCTURAL CHARACTERISATION

3.1.1 VISUAL APPEARANCE OF SAMPLES

Visual appearance during the attack indicates no major failure in any composition in the form of generalised spalling of the external surface or tensile splitting of the sample. The geometrical characteristics and specimen preparation adopted in this study prevented the development of failure modes that might compromise the interpretation of the macro-structural response of the material.

Figure 4 depicts the visual appearance of the external surface of the four compositions at the end of the test. In 0.38_8.1%, 0.45_12.4% and 0.55_13.7%, a thin, dense layer covering most of the surface was observed. This layer appeared in small localised regions approximately in the second month of exposure and spread at different rates until the end of the test. Samples with lower water/cement ratio (0.38_8.1% and 0.45_12.4%) showed the higher formation rates. As a result, these samples experienced localised spalling in locations within the region covered by the layer. In Figure 4, these locations are highlighted with a red circle.

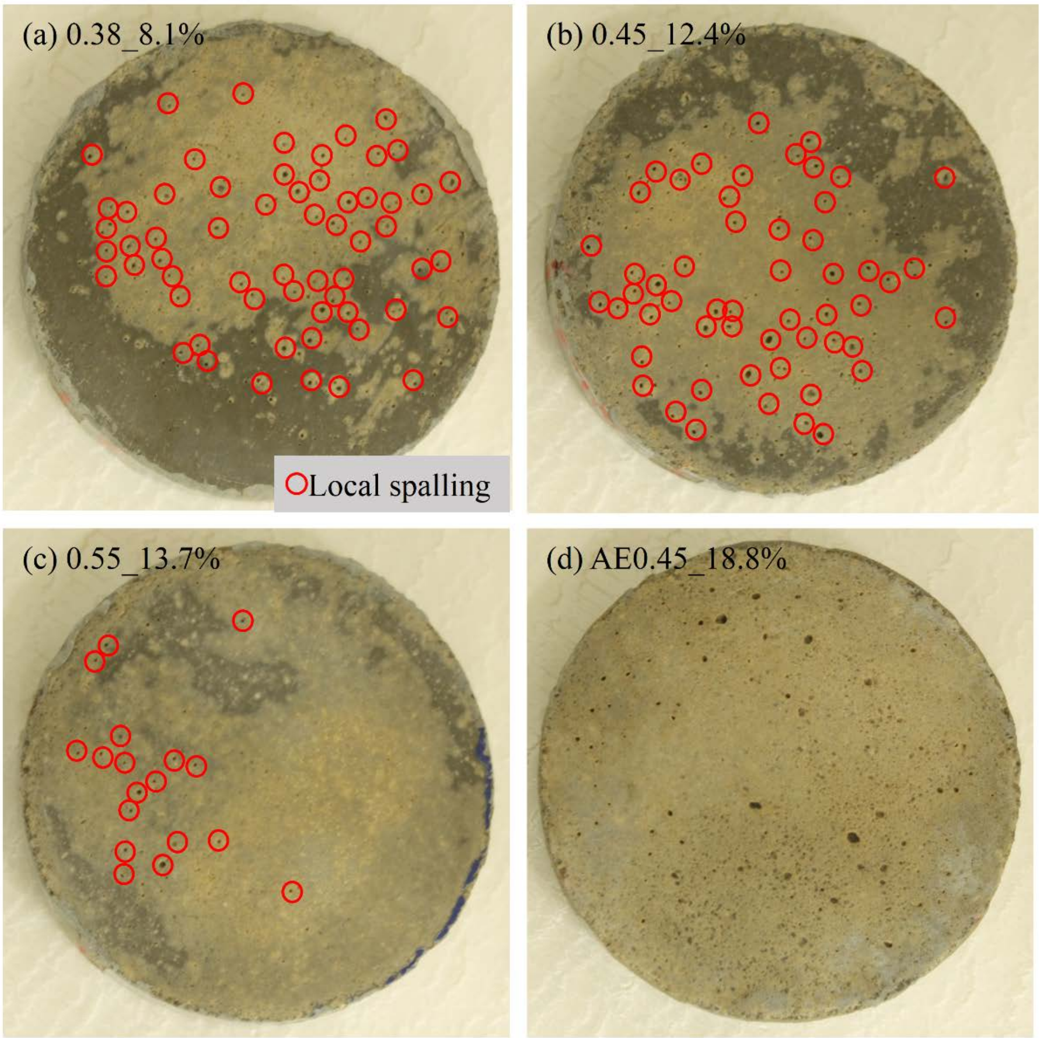

A comparison of the amount of red circles between Figure 4a, 4b and 4c clearly indicates that the physical damage in the form of local spalling increases with the decrease of the porosity of the samples. This observation concurs with the results presented by Naik et al. [14]. On the other hand, in mortars with air entrained (Figure 4d) this dense layer is not visible at any stage of the attack.

3.1.2 EXPANSIONS

Figure 5 depicts the radial expansion of the mortars during the 365 days of sulphate exposure. In order to distinguish the effects of sulphate exposure from the normal hydration process, data presented in Figure 5 corresponds to the difference between exposed and control specimens. Due to the large number of measuring points at each curve, +1/-1 standard deviation bars are only depicted at 28, 90, 180, 270 and 365 days. The maximum, minimum and mean standard deviation of all radial expansion measurements are $1.28\cdot10^{-4}$, $2.36\cdot10^{-5}$ and $5.71\cdot10^{-5}$ respectively. Results for 0.38_8.1%, 0.45_12.4% and 0.55_13.7% series show a first stage of rapid expansions followed by a second stage characterised by a decrease in the expansion rate. In the case of 0.55_13.7%, this decrease is considerably less pronounced than in the other compositions. The duration of the first stage is approximately 77, 63 and 25 days respectively for 0.38_8.1%, 0.45_12.4% and 0.55_13.7%, as indicated by the vertical lines on each expansion curve (duration estimated by the first consecutive measure where the expansion increase is below 5%).

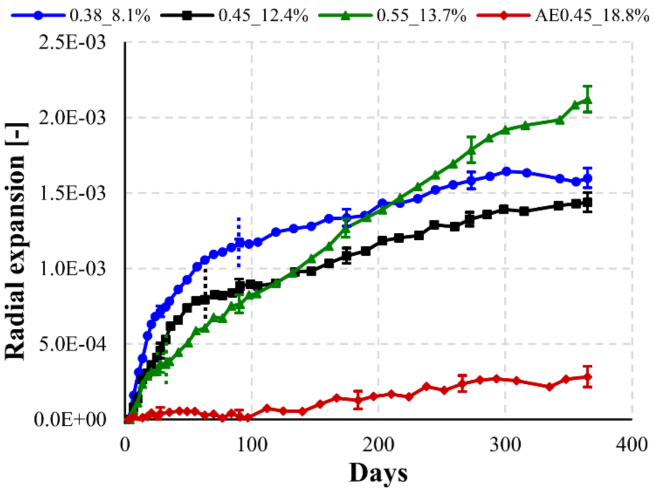

The first stage may be caused by the high initial sulphate concentration gradient between the solution outside and inside the specimen. Moreover, the early exposure facilitates sulphate ingress due to the low densification of the matrix at this moment. Therefore, a sudden sulphate concentration boost in the pore solution of the matrix close to the surface should be observed. This may cause ettringite precipitation and crystallisation pressure increase at locations where calcium, aluminium and sulphates meet. According to the prescriptions included in codes, the magnitude of the expansions should be more evident in the compositions with higher porosity, as the penetration is presumably enhanced. However, Figure 5 shows the opposite trend for the first stage of the expansion curve, as mortar 0.38_8.1% presents the highest expansions but the lowest porosity.

This behaviour might be explained by a retardation of the cement hydration derived from the different dosages of superplasticiser adopted in the compositions. This may lead to higher initial porosities in the matrices with higher dosages (0.38_8.1%), prior to the first porosity measurement performed at 14 days. Even though this hypothesis is in line with the established knowledge on ESA included in codes, it presents several shortcomings. First, the effects on cement hydration from polycarboxylate superplasticisers are usually reported to alter up to 3 days of hydration [33]. Since the mortars were exposed to the sulphate solution 48h after casting, the effects of the superplasticiser on the pore structure should be minor. Moreover, it seems unlikely that these effects overcome the large difference on water contents introduced by the different water/cement ratios adopted. Finally, the trends described are consistent after the first porosity measurement (at 14 days of exposure), where it is confirmed that the decrease of water/cement ratio leads to a reduction of porosity.

Alternatively, it is believed that in this stage expansions are defined by the capacity of the matrix to accommodate expansive products. In refined pore networks, the initial sulphate concentration boost might cause sudden ettringite precipitation in small pores, as the dense matrix force the sulphate flux through small capillary pores before reaching larger pores. Due to the large availability of large pores in coarse pore networks, the precipitation could mainly occur in locations with a high capacity to accommodate expansive phases without creating expansion [15,16].

The decrease of expansion rates observed in the second stage for series 0.38_8.1%, 0.45_12.4% and 0.55_13.7% might be related to the kinetics of diffusion (reduction of concentration gradient) and the influence of a pore-filling effect in the diffusion coefficient of the external layers of the samples. Interestingly, the reduction of the expansion rate is also related to the porosity of the mortars. In this case, mortars with lower porosity (0.38_8.1% and 0.45_12.4%) show bigger reductions in the expansion rate in comparison with mortars with higher porosity (0.55_13.7%), which present lower decrease. A possible explanation is that in refined pore systems, the precipitation produced during the first stage severely hinders sulphate penetration later, thus decreasing the expansion rates. In porous matrices, the precipitation achieved is not enough to fill a significant fraction of the capillary pores. Consequently, the penetration rate should not be significantly altered and expansions would only be slightly reduced. This hypothesis explains the steady expansion of samples 0.55_13.7%.

The air-entrained mortar presents a particular evolution over time. For this series, no initial expansion is observed in the first stage, its onset only occurring after 100 days of exposure. However, the expansion rates observed are still smaller than in other compositions. The absence of expansions during the first 100 days could be related to the high capacity of the matrix to accommodate expansive product. Due to the extensive availability of large pores relative to the amount of ettringite formed, the pore-filling effect that hinders sulphate penetration described for the other compositions does not apply. As a result, instead of a reduction of expansions in the late stages of the attack, for this composition the expansion rate increased. In terms of the absolute values reached at the end of the accelerated test, the total expansion of the composition with air-entrainer is 7.5 times smaller than the composition with 0.55 water-cement ratio.

The profiles depicted in Figure 5 reflect the double role of porosity in ESA. To highlight this, Figure 6 shows the incremental radial expansion at different periods of exposure, with the error bars included in each column corresponding to a +1 standard deviation. During the first 28 days, results indicate that the capacity of the matrix to accommodate expansive product constitutes the main resistance mechanism against

ESA, as expansions decreases with the increment of porosity. However, from 90 days of exposure this trend is reversed for the non-air-entrained mortars, as expansions decrease with the decrease of porosity. Therefore, at this stage the permeability of the matrix is the main factor that define the behaviour against the attack. Notice that the air-entrained mortar shows the smallest increments of expansions in almost all periods evaluated. This result may indicate that the first stage where the buffer capacity of the matrix controls the overall resistance against the attack can be extended over time if a sufficient amount of large pores are available.

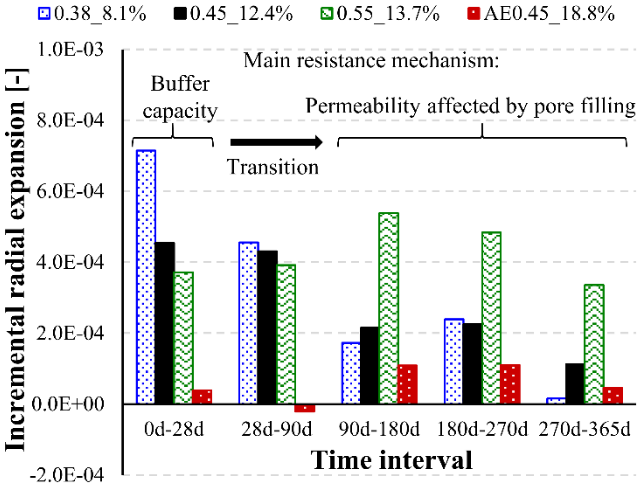

Figure 6 also sheds light on the reasons for the differences in behaviour found between mixes 0.38_8.1% and 0.45_12.4%. The higher final expansion of the former is justified by a significantly higher expansion in the period 0d-28d, which is approximately 57% greater than the observed in 0.45_12.4% at the same period. In later periods, both compositions show similar increments in radial expansion. Therefore, the bigger final expansion of 0.38_8.1% in comparison with that from 0.45_12.4% is possibly the consequence of a lower buffer capacity in the initial stages due to the more refined porosity.

3.1.3 ULTRASONIC PULSE VELOCITY

Figure 7 shows the evolution of the ultrasonic pulse velocity for the different compositions considered (difference between specimens stored in sulphate solution and control at a certain time divided by the difference at the beginning of the accelerated attack). Due to the large number of measuring points at each curve, +1/-1 standard deviation bars are only depicted at 28, 90, 180, 270 and 365 days. The maximum, minimum and mean standard deviation of all velocity change measurements are 2.35, 0.11 and 0.76 % respectively. Changes in velocity can be possibly related to the change in the density and integrity of the specimens. Positive values suggest denser matrices while negative values are indicative of damage. Samples from series 0.38_8.1%, 0.45_12.4% and 0.55_13.7% show similar trends with a decrease in ultrasonic velocity with exposure time. As described in Figure 5 for the expansion, the relative velocity change also depicts 2 stages. The first of these presents a rapid decrease of relative velocity indicating high degradation rates. After that, a deceleration of the degradation is observed, probably caused by the reduction of the penetration rate of sulphates due to the pore-filling effect and the decrease of the sulphate concentration gradient, as described in section 3.1.2. The differences observed amongst 0.38_8.1%, 0.45_12.4% and 0.55_13.7% should be evaluated with caution, specially at early ages, as the relatively high variability of the measurements might compromise analysis of the results.

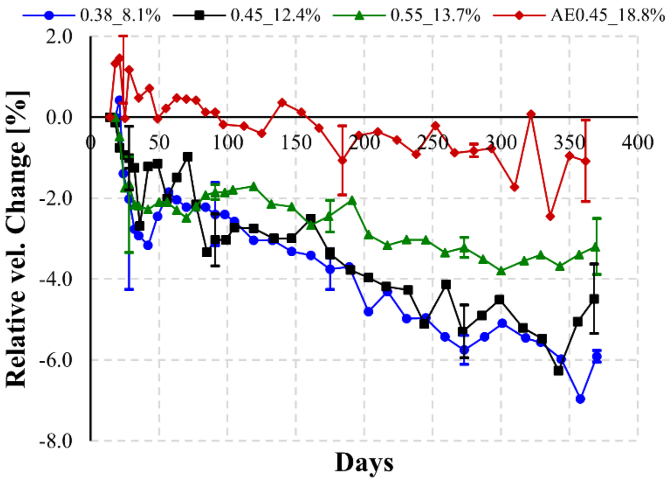

The evaluation of the velocity change at the end of the test shows that the degree of damage increased in inverse proportion to porosity. In fact, the composition with the denser matrix and smaller porosity (0.38_8.1%) presents the higher velocity reduction amongst all the compositions studied, indicating relatively higher damage caused by the attack. This result is in line with the visual inspection performed in section 3.1.1, but is not consistent with the expansion profiles presented in 3.1.2 (at the end of the test, 0.38_8.1% did not show the highest dimensional variation). Such results could be explained by the reduced extensibility of the material due to higher stiffness of the denser matrix [14]. Therefore, even though a relatively higher damage occurs, the higher elastic modulus restrains the deformation, leading to the assessment of lesser expansion.

Air-entrained mortars (AE0.45_18.8%) meanwhile maintained similar velocities than the control specimens throughout the accelerated attack, indicating low levels of damage. These results are in line with the expansion curves presented in Figure 5, where AE0.45_18.8% mortars exhibited the lowest expansions amongst all compositions.

3.1.4 MASS EVOLUTION

Figure 8 depicts the relative mass variation over time for all mortars studied. In order to isolate the effects of sulphate exposure from the phenomena of absorption, hydration and leaching experienced by all samples, this figure represents the differences between exposed and control specimens. Due to the large number of measuring points at each curve, +1/-1 standard deviation bars are only depicted at 28, 90, 180, 270 and 365 days. The maximum, minimum and mean standard deviation of all relative mass change measurements are 0.033, 0.003 and 0.011 % respectively. Notice that most error bars are barely visible in the graph due to the low variability of the results. Despite the fact that all samples presented a slight positive mass change, mortars subject to sulphate exposure showed a much lower mass increase. Therefore, Figure 8 shows negative mass variations for all compositions. Up to 200 days, sulphate exposure causes higher mass reduction as porosity increases, while the mass of 0.38_8.1%, 0.45_12.4% and AE0.45_18.8% mortars continues to decrease over time. However, 0.55_13.7% series presents a change in tendency, showing a mass increase after 200 days.

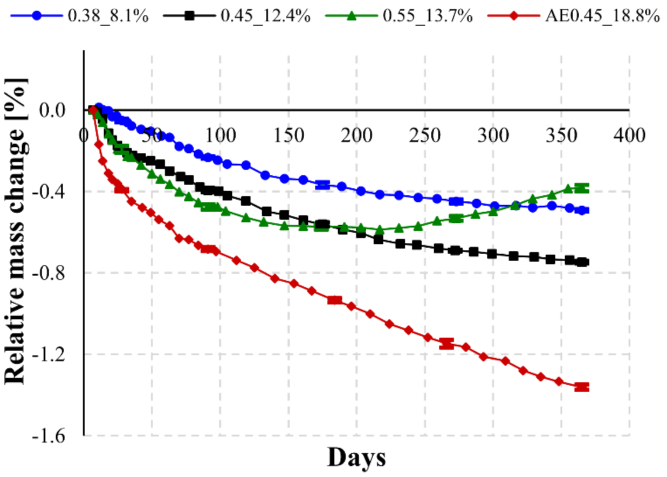

The mass reduction due to sulphate exposure could be explained by several processes occurring after sample immersion. Mortars in the aggressive media experience sulphate uptake from the external solution, which causes an increment of mass. However, sulphate ingress triggers a series of chemical reactions that involves dissolution of soluble calcium bearing phases for ettringite and gypsum precipitation. To maintain the equilibrium of the system, hydroxide ions released from portlandite dissolution diffuse towards the external solution, causing mass reduction. Measures of pH at the end of the test confirm higher leaching rates in the mortars submerged in the Na_2SO_4 solution compared to control (9.46 and 8.73, respectively), while calcium content by ICP-OES at the end of the test also indicates that calcium leaching phenomenon is more pronounced in the aggressive solutions (88.37 ppm over 56.06 ppm). These phenomena should be intensified as porosity and permeability of the specimen increases, in line with the initial trends depicted in Figure 8.

The slope reduction shown by non-air-entrained mortars at later stages of the attack indicates a deceleration of the leaching process, which could be explained by lower concentration gradients between external and internal solutions and the pore-filling effect caused by the precipitation of phases in the superficial pores of the specimens. As described in Figure 4, non-air-entrained mortars present a thin dense external layer that might slow down the leaching process. On the other hand, this dense layer is not visible in AE0.45_18.8% series, which could explain why in this composition the leaching phenomenon seems to progress at a similar rate until the end of the test. The particularly high mass gain experienced by 0.55_13.7% from 200 days on could be explained by a macroscopic swelling caused by the large expansions measured. Notice that this age corresponds to the age when the expansion of this series becomes the highest amongst all compositions studied (see Figure 5).

The physical changes observed here suggest that the role of the pore network during ESA is not only related to the transport process and the amount of expansive phases formed. According to the results obtained, the buffer capacity of the matrix to accommodate the product precipitated might be more relevant than the permeability itself when it comes to define the durability of the specimens at early stages of the attack.

3.2 MICRO-STRUCTURAL ANALYSIS

3.2.1 XRD ANALYSIS

This section presents the evolution of phase composition measured by quantitative XRD analysis for the different compositions during sulphate exposure. To simplify the interpretation of the results, only crystalline phases interacting with the sulphate ions are presented and phase contents are expressed as a percentage of the cement content.

Figure 9 depicts ettringite, gypsum and portlandite contents for all compositions at the end of the test. The sum of expansive phases (ettringite and gypsum) range between 14.3 % in the composition with 0.38 water/cement ratio and 29.9 % in the air-entrained mortars. On the other hand, Portlandite contents only present a slight variation, with values between 14.0 % and 17.6 % for 0.38_8.1% and AE0.45_18.8%, respectively. As expected, Rietveld quantification reveals increasing amounts of expansive phases with the increase of porosity of the composition, with results suggesting that the pore system affects the sulphate penetration rate of each composition, causing precipitation of different amounts of expansive products.

Figure 9 also includes the radial expansions measured at 365 days with its corresponding +1/-1 standard deviation bars. Results indicate no clear relationship between the amounts of expansive phases and the final radial expansions measured. Although the amount of expansive phases in AE0.45_18.8% is 2.1 times bigger than in 0.38_8.1%, the final radial free expansion obtained decreases by a factor of 5.7.

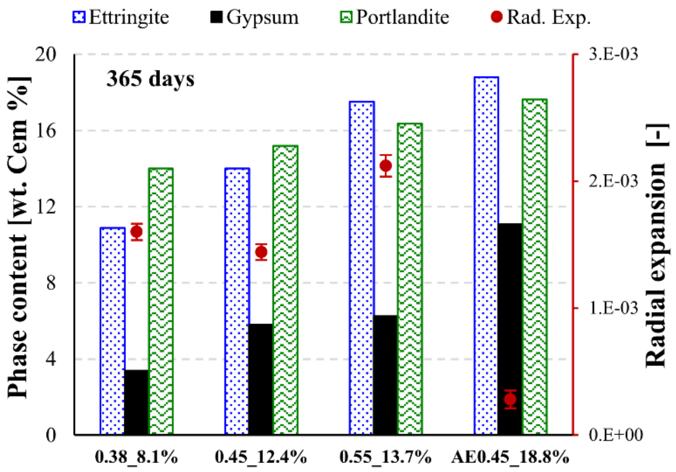

In order to further evaluate the relationship between expansive phases and expansions at different stages of the attack, Figure 10 shows the evolution of ettringite, gypsum and portlandite contents combined with the radial expansions for 0.45_12.4% and AE0.45_18.8% mortars at 28, 90, 180, 270 and 365. These compositions were selected for presenting the same water/cement ratio and aggregate content, with the main difference the presence of air voids intruded by the air-entraining agent. Both compositions already show high ettringite and gypsum contents after 28 days of exposure.

After that, 0.45_12.4% depicts similar contents until the end of the test (-0.1 % between 28 and 365 days) while AE0.45_18.8% shows a moderate increase (+8.9 % between 28 and 365 days). In both cases, the increments of expansion and the amount of expansive phases formed during the same period do not seem to present any direct relationship at any stage of the attack. Series 0.45_12.4% clearly illustrates this statement. Even though expansion increases by $9.8 \cdot 10^{-4}$ between 28 and 365 days, the amount of expansive phases remain almost unaltered. Again, this suggests that the progressive precipitation of expansive phases consumes part of the buffering capacity of the pore system. Once the buffering capacity is reduced, precipitations of even small amounts of expansive phases lead to significant expansion.

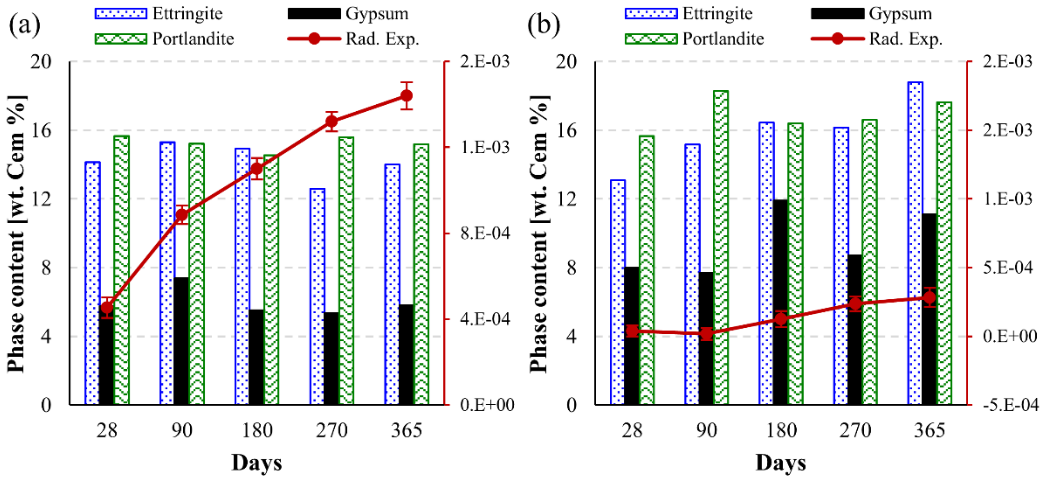

ESA-related expansions have traditionally been attributed to the additional volume generated by ettringite formation. Therefore, dimensional variations should imply the precipitation of expansive phases. However, the results obtained depicts no clear link between these two variables. This is in agreement with other studies of the literature [34,35] that did not find any clear correlation between the amount of ettringite formed and the expansions observed. Amongst the other possible ESA expansion mechanisms that have been suggested in the literature [2], the crystallisation pressure theory might be the only one that could explain the results obtained.

This theory states that expansions are originated from the crystallisation pressure developed by ettringite formation in a supersaturated pore solution [4,5,36]. According to this theory, only ettringite formed in small pores is likely to generate enough pressure to cause damage [34]. During the initial stages of exposure, there is rapid increase of sulphate content in the pore network causing the early precipitation of expansive phases. Due to the extremely high concentration of sulphates and the inability to generate enough ettringite to reduce the degree of supersaturation in regions with a very refined matrix, there is a crystallisation pressure boost at these locations. This pressure is responsible for the degradation and damage observed during the first stage of the attack (Figures 5 and 7). At later stages, due to a lower penetration rate caused by the pore-filling effect, this excess of sulphate ions can be allocated to other locations, more thermodynamically stable, with a consequent decrease in crystallisation pressure. This phenomenon is reflected on the macro-scale by a reduction of the expansions and degradation rates, as observed in Figures 5 and 7.

In the case of AE0.45_18.8%, the absence of expansions during the initial stage might be explained by the large availability of locations to accommodate the initial ettringite precipitated and sulphate excess without developing high crystallisation pressures. Unlike more refined matrices, the air-entrained mortars do not experience a significant reduction of sulphate penetration due to the pore-filling effect (Figure 1). Consequently, sulphate content continues to increase at a steady rate until crystallisation pressure starts to develop in some parts of the matrix. This phenomenon might explain the slight expansion and degradation observed after 150 days of exposure (Figures 5 and 7).

3.2.2 CHARACTERISATION OF THE PORE STRUCTURE

This section presents the results of a comprehensive analysis of the pore size distribution performed by MIP tests at 14, 28, 90, 180 and 270 days to obtain a qualitative picture of the evolution of the pore network throughout the attack. Figure 11 shows the evolution of the total volume of mercury intruded and MIP porosity for all mortars under sulphate exposure. The error bars included correspond to +1/-1 standard deviation. As expected, the volume intruded and porosity increases with increasing water/cement ratio and addition of an air-entrainer. Initial porosities at 14 days ranged between 8.1 % and 13.7 % for mortars with a water/cement ratio between 0.38 and 0.55. In air-entrained mortars, porosities of 18.8 % were observed due to the inclusion of air bubbles.

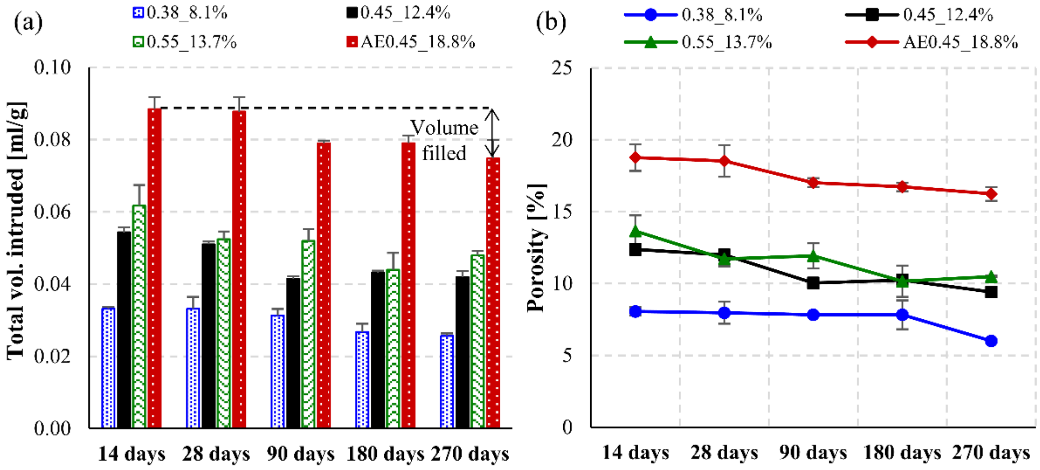

As the attack proceeds, the mercury intruded and porosity decrease as a result of normal cement hydration processes and the precipitation of expansive phases in the pore network. The difference between the total volume intruded at 14 and 270 days allows the assessment of the pore volume filled by these two phenomena in each composition. Mortars with higher porosity (0.55_13.7% or AE0.45_18.8%) display 1.8 times more pore volume filled than the composition 0.38_8.1%. This result suggests that both cement hydration and precipitation of expansive phases are more significant in compositions with higher porosities, in line with the XRD results shown in Figure 9.

However, the assessment of the fraction of volume filled from the initial total pore volume depicts different trends. In this case, 0.38_8.1% mortars show 1.5 times more ratio of volume filled than AE0.45_18.8% between 14 and 270 days. This result suggests that despite mortars with refined pore networks present lower precipitation of expansive phases and slower cement hydration, the volume filled represents a higher fraction of the total volume available. Therefore, in these compositions the pore-filling effect is more significant. These trends correspond to the visual inspection of the specimens described in section 3.1.1.

Figure 12 shows the evolution of the critical pore diameter for 0.38_8.1%, 0.45_12.4% and 0.55_13.7% under sulphate exposure at 14, 28, 90, 180 and 270 days, with the error bars included corresponding to +1 standard deviation. This semi-quantitative parameter can be usually related to the permeability of the material [20]. Results for AE0.45_18.8% series are not included as the air bubbles produce high increments of intrusion in large diameters which distort the assessment and hinder comparison with the other compositions.

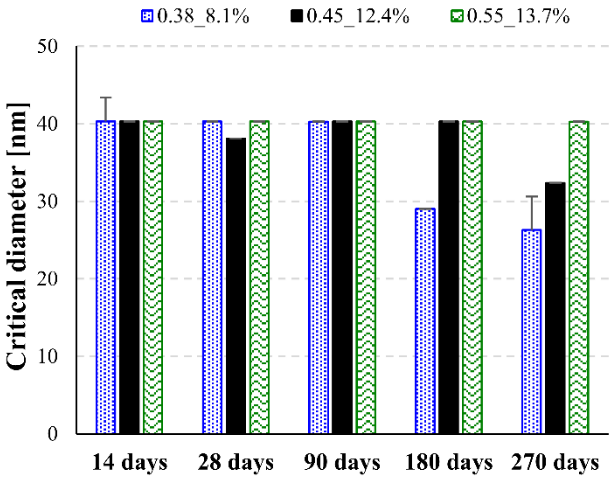

Despite the differences in porosity, non-air-entrained mortars present similar critical diameters until 90 days of exposure. After that, mortars with low water/cement ratios display an important reduction of critical diameter, with this trend becoming even more evident at the end of the evaluated period. The inability of the critical diameter to capture differences in the permeability during the early stages of the attack might be explained by the fact that this parameter does not account for the most accessible path for fluid transport in the cement paste but the mean pore size that allows maximum percolation. Results suggest that these pores might only be affected at late stages of the attack, when the most accessible paths are reduced due to the pore-filling effect and the formation of the thin layer described in section 3.1.1.

Figure 13 shows the evolution of the pore size distribution of all mortars according to 5 predefined pore ranges (<10 nm, 10-50 nm, 50-100 nm, 100-500 nm and >500 nm). The error bars included correspond to +1/-1 standard deviation. This figure shows how sulphate exposure alters the pore-size distribution of the material and allows a qualitative assessment of the precipitation patterns amongst the different compositions. The evolution of the different pore ranges between 14 and 270 days shows similar trends for the non-air-entrained mortars. For these compositions, the refinement of the pore network during the attack is mainly caused by the reduction of pores between 50 – 100 nm. This pore range accumulates the 63.0 %, 66.4 % and 58.2 % of the total volume filled by the combined action of cement hydration and precipitation of expansive phases in 0.38_8.1%, 0.45_12.4% and 0.55_13.7%, respectively. However, the AE0.45_18.8% series only accumulates 31.1 % of the volume filled in this pore range. In this case, the main reduction of intrusion is observed in pores of 100 - 500 nm, which concentrates the 60.4 % of the reduction.

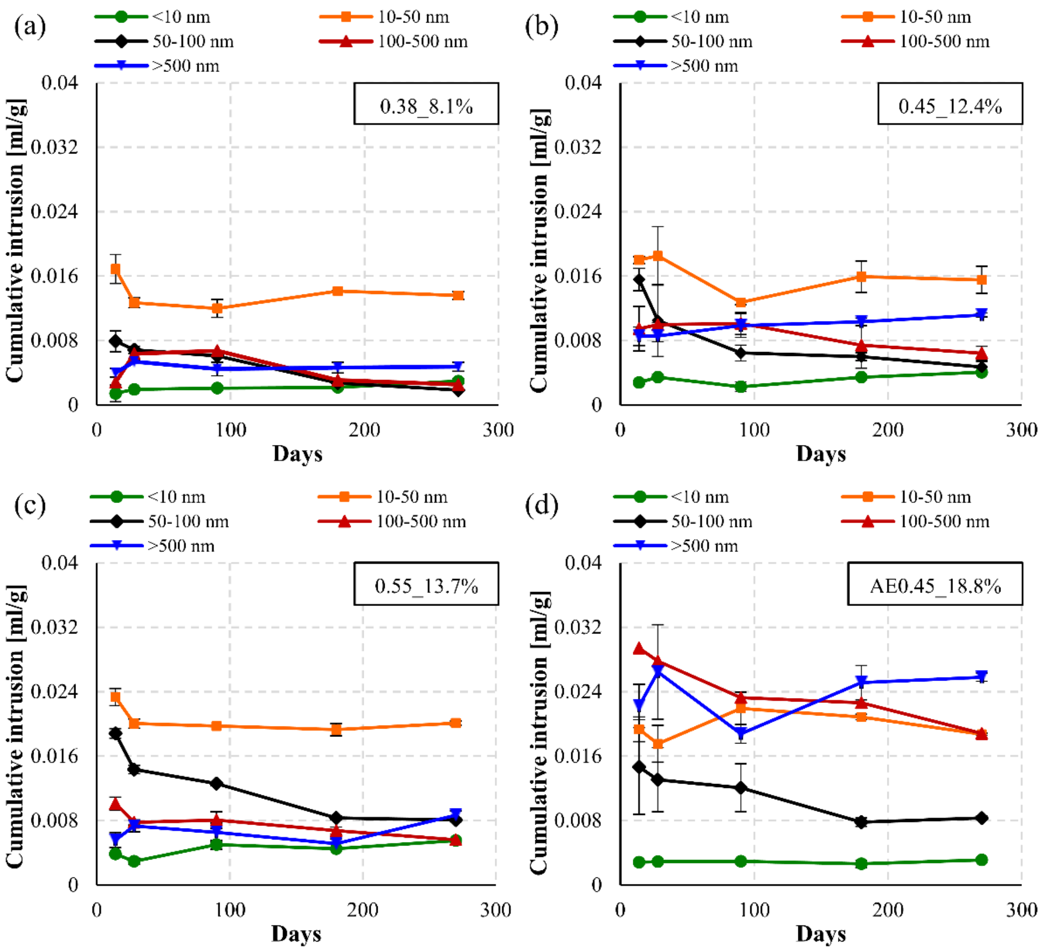

Although the pore sizes measured in the MIP technique do not necessarily match the real pore size distribution of the material, the qualitative analysis of the results highlight that the pore sizes affected during ESA vary depending on the characteristics of the pore system of the matrix. Results indicate that in air-entrained mortars, the alterations in the pore network are produced in bigger pore ranges than the observed in other compositions, which is in agreement with other studies [37]. The bigger pores of AE0.45_18.8 act as pressure releases that limit the pressure increase in the system, especially in smaller pores. This pressure release effect combined with the capacity to accommodate expansive phases might explain the lower degrees of damage observed in AE0.45_18.8.

4. CONCEPTUAL MODEL OF THE ROLE OF POROSITY

The approach adopted in the codes to obtain durable materials against ESA is based on a fairly simple perception of the role of the porosity. It assumes that the amount of ettringite precipitated defines the damage generated in the material. Therefore, codes prescribe materials with low permeability to reduce the penetration of sulphate ions.

However, this study shows that the amount of expansive phases itself is not always a good indicator of the level of deterioration. Sometimes, other aspects such as the location of the precipitation and the presence of pressure release pores might play a more significant role in the outcome of the attack.

The results obtained in this study highlight two mechanisms defined by the pore network that contribute to ESA resistance: permeability, which is related to the amount of expansive phases potentially generated, and buffer capacity, which might define the preferential location of the precipitation of expansive products. Overall ESA resistance defined by the pore network is the result of the contribution of these two mechanisms. Since the pore network characteristics do not remain constant over time (due to cement hydration and pore-filling effect), the contribution of these two mechanisms also varies during the attack.

Figure 14 represents this phenomenon in a schematic way. A material with low porosity achieves high durability by the low permeability of the matrix, which hinders sulphate ingress and potential ettringite precipitation. As porosity increases, sulphate penetration is promoted, thus reducing the durability of the material. The buffer capacity curve, however, shows an opposite trend. In this case, ESA resistance increases for high values of porosity due to a preferential precipitation in large pores and decreases along the refinement of the pore network. Notice that this model does not account for the effects of crack formation. The model depicted in Figure 14 therefore represents the role of porosity during the attack prior to the onset of cracking.

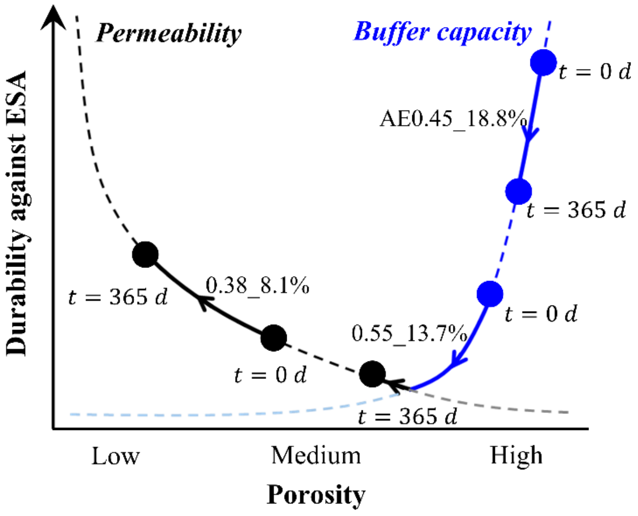

Figure 14 includes a qualitative location of 0.38_8.1%, 0.55_13.7% and AE0.45_18.8% based on the porosity of these compositions. 0.45_12.4% is not depicted for clarity in the interpretation of the graph. At early stages of the attack, 0.38_8.1% presents the lowest durability, which is reflected by displaying the largest expansions amongst the compositions evaluated (Figure 5). As time proceeds, the durability of this composition improves due to a reduction of porosity, which results in a decrease of the expansion rate.

Meanwhile, the air-entrained mortar initially presents the highest durability due to the large buffer capacity of the matrix (no expansions measured). Despite durability reduces over time as the precipitation of expansive phases reduce the buffer capacity, this composition keeps displaying the highest potential durability against ESA at the conclusion of the test. Finally, 0.55_13.7% mortars display a half-way behaviour with an initial stage characterised by a pore system that is capable of accommodating part of the expansive phases. A decrease in durability is caused by the precipitation of expansive phases that reduces the buffer effect of the porosity.

Further research on the use of air-entrainers with other mortar mixtures is recommended to validate the buffer capacity curve shown in Figure 14. The design of durable materials against ESA based on high buffer capacities should be made with caution. In these cases, durability tends to drop off over time as the pore-filling effect has a negative impact on the matrix buffer capacity, while the continuous formation of ettringite might lead to a significant strength-loss of the material due to decalcification of portlandite or C-S-H gel. The approach based on low permeability is safer however, as the pore-filling effect developed over time has a positive impact on permeability.

5. CONCLUSIONS

The following specific findings may be derived from this study.

- Expansion measurements suggest that the buffer capacity of the pore structure defines the damage developed during the early stages of ESA. After that, the transport process affected by the precipitation of expansive phases controls the durability. The duration of the first stage can be extended if sufficient number of large pores relative to the amount of ettringite formed are available in the material.

- Air-entrained mortars displayed the lowest expansion and ultrasonic-pulse velocity variation over time, possibly characterised by the smallest damage level amongst all compositions tested. MIP results suggest that this behaviour might be explained by a preferential precipitation of expansive phases in large pores, which buffers the pressure increase in the pore system and accommodates expansive phases without causing damage.

- Quantitative XRD analyses shows no direct relationship between the damage generated and the amount of expansive product formed during any stage of the attack. In fact, the biggest precipitation of expansive phases was found in the composition that presents the least expansion.

ACKNOWLEDGMENTS

Support from the Spanish Ministry of Economy and Competitiveness through research project BIA2013-49106-C2-1-R is greatly acknowledged. T. Ikumi is supported by the fellowship programme FPI BES-2014-068524 of the Spanish Ministry of Economy and Competitiveness.

REFERENCES

[1] M. Alexander, A. Bertron, N. De Belie, Performance of Cement-Based Materials in Aggressive Aqueous Environments, Springer, 2013.

[2] J.P. Skalny, I. Odler, J. Marchand, Sulfate Attack on Concrete, Spon, London, 2001.

[3] R. Tixier, B. Mobasher, Modeling of Damage in Cement-Based Materials Subjected to External Sulfate Attack. I: Formulation, J. Mater. Civ. Eng. 15 (2003) 305–313.

[4] G.W. Scherer, Stress from crystallization of salt, Cem. Concr. Res. 34 (2004) 1613-1624.

[5] R.J. Flatt, G.W. Scherer, Thermodynamics of crystallization stresses in DEF, Cem. Concr. Res. 38 (2008) 325-336.

[6] C. Yu, W. Sun, K. Scrivener, Mechanism of expansion of mortars immersed in sodium sulphate solutions, Cem. Concr. Res. 43 (2013) 105-111.

[7] F.P. Glasser, J. Marchand, E. Samson, Durability of concrete — Degradation phenomena involving detrimental chemical reactions, Cem. Concr. Res. 38 (2008) 226-246.

[8] A. Çavdar, S. Yetgin, Investigation of mechanical and mineralogical properties of mortars subjected to sulphate, Constr. Build. Mater. 24 (2010) 2231-2242.

[9] R. El-Hachem, E. Rozière, F. Grondin, A. Loukili, Multi-criteria analysis of the mechanism of degradation of Portland cement based mortars exposed to external sulphate attack, Cem. Concr. Res. 42 (2012) 1327-1335.

[10] W. Piasta, J. Marczewska, M. Jaworska, Durability of air entrained cement mortars under combined sulphate and freeze-thaw attack, Procedia Eng. 108 (2015) 55-62.

[11] T. Ikumi, S.H.P. Cavalaro, I. Segura, A. de la Fuente, A. Aguado, Simplified methodology to evaluate the external sulphate attack in concrete structures, Mater. Des. 89 (2016) 1147-1160.

[12] I. Oliveira, S.H.P. Cavalaro, A. Aguado, New kinetic model to quantify the internal sulphate attack in concrete, Cem. Concr. Res. 43 (2013) 95–104.

[13] T. Ikumi, S.H.P. Cavalaro, I. Segura, A. Aguado, Alternative methodology to consider damage and expansions in external sulphate attack modeling, Cem. Concr. Res. 63 (2014) 105-116.

[14] N.N. Naik, A.C. Jupe, S.R. Stock, A.P. Wilkinson, P.L. Lee, K.E. Kurtis, Sulfate attack monitored by microCT and EDXRD: Influence of cement type, water-to-cement ratio, and aggregate, Cem. Concr. Res. 36 (2006) 144-159.

[15] M. Santhanam, M.D. Cohen, J. Olek, Mechanism of sulphate attack: A fresh look Part 1: Summary of experimental results, Cem. Concr. Res. 32 (2002) 915-921.

[16] M. Santhanam, M.D. Cohen, J. Olek, Mechanism of sulphate attack: a fresh look Part 2. Proposed mechanisms, Cem. Concr. Res. 33 (2003) 341-346.

[17] A.E. Idiart, C.M. López, I. Carol, Chemo-mechanical analysis of concrete cracking and degradation due to external sulphate attack: A meso-scale model, Cem. Concr. Compos. 33 (2011) 411-423.

[18] R. El-Hachem, E. Rozière, F. Grondin, A. Loukili, New procedure to investigate external sulphate attack on cementitious materials, Cem. Concr. Compos. 34 (2012) 357-364.

[19] A. Chabrelie, Mechanisms of degradation of concrete by external sulphate ions under laboratory and field conditions, PhD Thesis, ÉPFL, Lausanne, 2010.

[20] I. Segura, Caracterización del proceso de descalcificación en morteros, mediante ensayos destructivos y no destructivos, PhD Thesis, ETSICCP, Madrid, 2008.

[21] D. Jansen, F. Goetz-Neunhoeffer, C. Stabler, J. Neubauer, A remastered external standard method applied to the quantification of early OPC hydration, Cem. Concr. Res. 41 (2011) 602-608.

[22] D. Jansen, C. Stabler, F. Goetz-Neunhoeffer, S. Dittrich, J. Neubauer, Does Ordinary Portland Cement contain amorphous phase? A quantitative study using an external standard method, Powder Diffract. 26 (2011) 31-38.

[23] R. Snellings, A. Bazzoni, K. Scrivener, The existence of amorphous phase in Portland cements: Physical factors affecting Rietveld quantitative phase analysis, Cem. Concr. Res. 59 (2014) 139-146.

[24] A.G. de la Torre, S. Bruque, J. Campo, M.A.G. Aranda, The superstructure of C3S from synchrotron and neutron powder diffraction and its role in quantitative analysis, Cem. Conc. Res. 32 (2002) 1347-1356.

[25] W.G. Mumme, R.J. Hill, G.W. Bushnell, E.R. Segnite, Rietveld crystal structure refinements, crystal chemistry and calculated powder diffraction data for the polymorphs of dicalcium silicate and related phases, N. Jb. Miner. Abh. (J. Min. Geochem.) 169 (1995) 35-68.

[26] H.E. Petch, The hydrogen positions in portlandite, Ca(OH)2, as indicated by the electron distribution, Acta Crystallogr. 14 (1961) 950-957.

[27] R. Wartchow, Datensammlung nach der ‘‘learnt profile”-methode(LP) für calcit und vergleich mit der ‘‘background peak background”-methode (BPB), Z. Kristallogr. 186 (1989) 300-302.

[28] F. Goetz-Neunhoeffer, J. Neubauer, Refined ettringite structure for quantitative X-ray diffraction analysis, Powder Diffr. 21 (2006) 4-11.

[29] W.A. Wooster, On the crystal structure of gypsum CaSO4(H2O)2, Z. Kristallogr. 94 (1936) 375-396.

[30] A.A. Colville, S. Geller, The crystal structure of brownmillerite, Ca2FeAlO5, Acta Crystallogr. B 27 (1971) 2311-2315.

[31] L. Levien, C.T. Prewitt, D.J. Weidner, Structure and elastic properties of quarz at pressure, Am. Mineral. 65 (1980) 920-930.

[32] E.N. Maslen, V.A. Streltsov, N.R. Streltsova, N. Ishizawa, Y. Satow, Synchrotron X-ray study of the electron density in alpha-Al2O3, Acta Crystallogr. B 49 (1993) 973-980.

[33] E. Sakai, T. Kasuga, T. Sugiyama, K. Asaga, M. Daimon, Influence of superplasticizers on the hydration of cement and the pore structure of hardened cement, Cem. Concr. Res. 36 (2006) 2049-2053.

[34] W. Müllauer, R.E. Beddoe, D. Heinz, Sulfate attack expansion mechanisms, Cem. Concr. Res. 52 (2013) 208-215.

[35] W. Kunther, B. Lothenbach, K. Scrivener, On the relevance of volume increase for the length changes of mortar bars in sulphate solutions, Cem. Concr. Res. 46 (2013) 23-29.

[36] C. Yu, W. Sun, K. Scrivener, Degradation mechanism of slag blended mortars immersed in sodium sulphate solution, Cem. Concr. Res. 72 (2015) 37-47.

[37] T. Ikumi, I. Segura, S.H.P. Cavalaro, Influence of early sulphate exposure on the pore network development of mortars, Constr. Build. Mater. 143 (2017) 33-47.